

Cite this: *Dalton Trans.*, 2018, **47**,  
2628

# Tin(IV) chalcogenoether complexes as single source precursors for the chemical vapour deposition of SnE<sub>2</sub> and SnE (E = S, Se) thin films†

Chitra Gurnani,<sup>a</sup> Samantha L. Hawken,<sup>b</sup> Andrew L. Hector,<sup>b</sup> Ruomeng Huang,<sup>b</sup> Marek Jura,<sup>d</sup> William Levason,<sup>b</sup> James Perkins,<sup>b</sup> Gillian Reid<sup>b</sup> \*<sup>b</sup> and Gavin B. G. Stenning<sup>d</sup>

The molecular Sn(IV) complexes, [SnCl<sub>4</sub>{<sup>n</sup>BuS(CH<sub>2</sub>)<sub>3</sub>S<sup>n</sup>Bu}] (**2**), [SnCl<sub>4</sub>{<sup>n</sup>Bu<sub>2</sub>S}] (**3**) and [SnCl<sub>4</sub>{<sup>n</sup>Bu<sub>2</sub>Se}] (**4**) have been prepared in good yield from reaction of SnCl<sub>4</sub> with the appropriate chalcogenoether ligand in anhydrous hexane and, together with the known [SnCl<sub>4</sub>{<sup>n</sup>BuSe(CH<sub>2</sub>)<sub>3</sub>Se<sup>n</sup>Bu}] (**1**), employed as single source precursors for the low pressure chemical vapour deposition of the corresponding tin dichalcogenide thin films. At elevated temperatures the bidentate ligand precursors, (**1**) and (**2**), also form the tin monochalcogenides, SnSe and SnS, respectively. In contrast, (**3**) gave a mixture of phases, SnS<sub>2</sub>, Sn<sub>2</sub>S<sub>3</sub> and SnS and (**4**) gave SnSe<sub>2</sub> only. The morphologies, elemental compositions and crystal structures of the resulting films have been determined by scanning electron microscopy, energy dispersive X-ray spectroscopy, grazing incidence X-ray diffraction and Raman spectroscopy. Van der Pauw measurements on the SnS<sub>2</sub>, SnS and SnSe<sub>2</sub> films confirm their resistivities to be 2.9(9), 266(3) and 4.4(3) Ω cm, respectively.

Received 12th October 2017,  
Accepted 10th November 2017

DOI: 10.1039/c7dt03848h

rsc.li/dalton

## Introduction

Tin chalcogenides (SnE<sub>x</sub>) (E = S, Se; x = 1, 2) are layered semi-conducting materials that are becoming widely acknowledged as important for a wide variety of electronic applications; specifically optoelectronics,<sup>1–5</sup> thermoelectrics<sup>6,7</sup> and phase change devices.<sup>8,9</sup> SnS<sub>2</sub> also shows potential for use in photo-detectors, with a high external quantum efficiency of 3.2 × 10<sup>5</sup>%;<sup>1</sup> high performance sodium storage, with a high reversible capacity reported of 576 mA h g<sup>−1</sup>;<sup>10</sup> and phototransistors with a high on/off ratio reported of >10<sup>6</sup>.<sup>2</sup> SnS, on the other hand, has a very low thermal conductivity ~0.29 W mK<sup>−1</sup> and a reported ZT value of 0.41,<sup>7</sup> which are of particular interest for thermoelectric devices, whilst ZT values as high as 2.6 have been claimed for single crystals of SnSe.<sup>7</sup> SnSe<sub>2</sub> has attracted

interest as a potentially effective phase change material for data storage applications. For this application fast recrystallisation times are key and SnSe<sub>2</sub>, with a recrystallisation time of 20 ns,<sup>9</sup> is a promising material in this field.

Tin chalcogenide thin films can be produced by a variety of methods. Using atmospheric pressure chemical vapour deposition and a dual source precursor approach, SnCl<sub>4</sub> with either H<sub>2</sub>S or Et<sub>2</sub>Se can produce SnS<sub>2</sub> or SnS,<sup>11,12</sup> and SnSe<sub>2</sub> or SnSe,<sup>13</sup> respectively, depending on the conditions employed. A single source precursor approach, in which the metal and chalcogen are incorporated into one molecular compound, can lead to easier to handle precursors (since they are coordinatively saturated), potentially easier control of stoichiometry and, in some cases, the ability to deposit the binary material selectively onto specific regions of a patterned substrate on the micro-<sup>14</sup> or nano-scale.<sup>15</sup> While this substrate selectivity is rather atypical of CVD, it can be highly advantageous for certain applications.

In previous work, SnS and SnS<sub>2</sub> have been produced from the tin(IV) thiolate complex, [Sn(SCH<sub>2</sub>CH<sub>2</sub>S)<sub>2</sub>], using aerosol assisted chemical vapour deposition in the presence of H<sub>2</sub>S gas,<sup>16</sup> or using alkyl tin dithiocarbamates<sup>17</sup> and SnS nanosheets by liquid exfoliation.<sup>18</sup> Single source precursor approaches to tin sulfide and selenide thin films by us have used the thio- and seleno-ether complexes, [SnCl<sub>4</sub>{*o*-C<sub>6</sub>H<sub>4</sub>(CH<sub>2</sub>EMe)<sub>2</sub>}] (E = S, Se)<sup>19</sup> to produce SnS<sub>2</sub> and small amounts of SnS and SnSe, or; [SnCl<sub>4</sub>(SeEt<sub>2</sub>)<sub>2</sub>]<sup>19</sup> and [SnCl<sub>4</sub>{<sup>n</sup>BuSe

<sup>a</sup>School of Natural Sciences, Mahindra Ecole Centrale, Hyderabad, India<sup>b</sup>Chemistry, University of Southampton, Southampton SO17 1BJ, UK.

E-mail: G.Reid@soton.ac.uk

<sup>c</sup>Electronic and Computer Science, University of Southampton, Southampton SO17 1BJ, UK<sup>d</sup>ISIS Neutron and Muon Source, Rutherford Appleton Laboratory, Harwell Science and Innovation Campus, Didcot, OX11 0QX, UK†Electronic supplementary information (ESI) available: <sup>1</sup>H, <sup>13</sup>C{<sup>1</sup>H}, <sup>77</sup>Se{<sup>1</sup>H} and <sup>119</sup>Sn NMR and IR spectroscopic data for each of the new complexes, together with their TGA profiles, EDX analyses for the SnE<sub>2</sub> and SnE films and SEM, XRD and Raman spectra for the films obtained by LP CVD using (**3**) at elevated temperature. See DOI: 10.1039/c7dt03848h

$(\text{CH}_2)_x\text{Se}^n\text{Bu}]$  ( $x = 2, 3$ )<sup>20</sup> to form  $\text{SnSe}_2$ . Within the chalcogen-oether- and chalcogenolate-based precursors, terminal butyl substituents have been shown to be well-suited for the growth of high quality binary chalcogenide thin films. This is attributed to their clean, low energy  $\beta$ -hydride elimination pathway.

Here we report the synthesis, characterisation and evaluation of three novel single source precursors,  $[\text{SnCl}_4\{\text{BuS}(\text{CH}_2)_3\text{S}^n\text{Bu}\}]$  (2) and  $[\text{SnCl}_4\{\text{Bu}_2\text{E}\}_2]$  ( $\text{E} = \text{S}$ , (3);  $\text{E} = \text{Se}$ , (4)), and their use for the low pressure chemical vapour deposition (LPCVD) of  $\text{SnS}_2$  and  $\text{SnSe}_2$  thin films, as well as variation of the deposition conditions to produce  $\text{SnSe}$  and  $\text{SnS}$  films. High temperature LPCVD using  $[\text{SnCl}_4\{\text{BuSe}(\text{CH}_2)_3\text{Se}^n\text{Bu}\}]$ , (1), is also explored as a route to  $\text{SnSe}$  films.

Energy dispersive X-ray (EDX), scanning electron microscopy (SEM), Raman spectroscopy and grazing incidence X-ray diffraction (XRD) data on the resulting films are presented, together with resistivities determined by van der Pauw measurements.

## Experimental

### Precursor preparation and characterisation

All reactions were conducted using Schlenk, vacuum line and glove box techniques under a dry nitrogen atmosphere. The reagents were stored and manipulated using a glove box. Hexane was dried by distillation over sodium wire.  $\text{SnCl}_4$ ,  $^n\text{BuLi}$  (1.6 mol  $\text{dm}^{-3}$  in diethyl ether) and  $^n\text{Bu}_2\text{S}$  were obtained from Sigma-Aldrich.  $^n\text{Bu}_2\text{S}$  was dried over sieves,  $\text{SnCl}_4$  and  $^n\text{BuLi}$  were used as received.  $^n\text{Bu}_2\text{Se}$ ,<sup>21</sup>  $^n\text{BuSe}(\text{CH}_2)_3\text{Se}^n\text{Bu}^{20}$  and  $[\text{SnCl}_4\{\text{BuSe}(\text{CH}_2)_3\text{Se}^n\text{Bu}\}]^{20}$  (1) were prepared according to the literature methods. IR spectra were recorded as Nujol mulls between CsI plates using a PerkinElmer Spectrum 100 instrument.  $^1\text{H}$  and  $^{13}\text{C}\{^1\text{H}\}$  NMR spectra were recorded from solutions in  $\text{CDCl}_3$  or  $\text{CD}_2\text{Cl}_2$  on a Bruker AV400 spectrometer,  $^{77}\text{Se}\{^1\text{H}\}$  and  $^{119}\text{Sn}$  NMR spectra on a Bruker AV400-II spectrometer and referenced to external neat  $\text{SeMe}_2$  and  $\text{SnMe}_4$  respectively. A small amount of  $[\text{Cr}(\text{acac})_3]$  was added as a relaxation agent to the samples for  $^{119}\text{Sn}$  NMR measurements. Microanalytical results were obtained from Medac Ltd.

$^n\text{BuS}(\text{CH}_2)_3\text{S}^n\text{Bu}$ : was obtained by dissolving  $\text{HS}(\text{CH}_2)_3\text{SH}$  (6.05 g, 56 mmol) in anhydrous EtOH (60 mL) with addition of elemental sodium (2.8 g, 112 mmol) cut into small pieces. After dissolution of the sodium, the reaction mixture was refluxed for 1 h, cooled to ambient temperature and  $^n\text{BuBr}$  (15.34 g, 12.03 mL, 112 mmol) was added slowly. The reaction mixture was then refluxed for 1 h, forming a white solid. After cooling, saturated aqueous NaCl and  $\text{NaHCO}_3$  solutions were added. After filtering, the product was extracted from the aqueous filtrate with  $\text{Et}_2\text{O}$  ( $4 \times 50$  mL), dried overnight ( $\text{Na}_2\text{SO}_4$ ) and, after removal of the drying agent, the solvent was removed *in vacuo*, leaving a colourless oil. Yield: 6.0 g, 48%.  $^1\text{H}$  NMR ( $\text{CDCl}_3$ , 298 K)  $\delta$ /ppm: 0.92 (t, [6H],  $\text{CH}_3$ ), 1.41 (m, [4H],  $-\text{CH}_2\text{CH}_3$ ), 1.57 (m, [4H],  $-\text{SCH}_2\text{CH}_2\text{CH}_2\text{CH}_3$ ), 1.86 (m, [2H],  $-\text{SCH}_2\text{CH}_2\text{CH}_2\text{S}-$ ), 2.52 (t, [4H],  $\text{SCH}_2-$ ), 2.62 (t, [4H],

$\text{SCH}_2-$ ).  $^{13}\text{C}\{^1\text{H}\}$  NMR ( $\text{CDCl}_3$ , 298 K)  $\delta$ /ppm 13.65 ( $\text{CH}_3$ ), 21.98, 29.43, 30.96, 31.74, 31.81 (all  $\text{CH}_2$ ).

$[\text{SnCl}_4\{\text{BuS}(\text{CH}_2)_3\text{S}^n\text{Bu}\}]$  (2). A solution of  $^n\text{BuS}(\text{CH}_2)_3\text{S}^n\text{Bu}$  (0.24 g, 1.09 mmol) in anhydrous hexane (5 mL) was added slowly to a solution of  $\text{SnCl}_4$  (0.15 mL, 1.25 mmol) in anhydrous hexane (10 mL) under constant stirring at room temperature and under a dinitrogen atmosphere. A white solid immediately precipitated out of solution. It was collected by filtration after 20 minutes and dried *in vacuo* to afford a white solid. Yield: 0.46 g, 88%. Anal. calcd for  $\text{C}_{11}\text{H}_{24}\text{Cl}_4\text{S}_2\text{Sn}$ : C 27.5, H 5.0. Found: C 26.9, H 5.3%.  $^1\text{H}$  NMR ( $\text{CDCl}_3$ , 298 K)  $\delta$ /ppm: 0.98 (t, [6H],  $\text{CH}_3$ ), 1.49 (m, [4H],  $\text{CH}_2\text{CH}_3$ ), 1.76 (m, [4H],  $\text{CH}_2$ ), 2.39 (m, [2H],  $-\text{SCH}_2\text{CH}_2\text{CH}_2\text{S}-$ ), 3.17 (m, [4H],  $\text{SCH}_2$ ), 3.32 (m, [4H],  $\text{SCH}_2$ ).  $^{13}\text{C}\{^1\text{H}\}$  NMR ( $\text{CDCl}_3$ )  $\delta$ /ppm: 13.50 ( $\text{CH}_3$ ), 21.87 ( $\text{CH}_2$ ), 24.02 ( $\text{CH}_2$ ), 29.40 ( $\text{CH}_2$ ), 34.19 ( $\text{CH}_2$ ), 36.74 ( $\text{CH}_2$ ).  $^{119}\text{Sn}$  NMR ( $\text{CH}_2\text{Cl}_2/\text{CD}_2\text{Cl}_2$ , 298 K):  $-575$  (br); (200 K)  $\delta$ /ppm:  $-567$ ,  $-585$ . IR (Nujol)  $\nu/\text{cm}^{-1}$ : 324 (s br) Sn–Cl.

$[\text{SnCl}_4\{\text{Bu}_2\text{S}\}_2]$  (3). A solution of  $^n\text{Bu}_2\text{S}$  (0.944 g, 6.45 mmol) in anhydrous hexane (5 mL) was added slowly to a solution of  $\text{SnCl}_4$  (0.840 g, 3.22 mmol) in anhydrous hexane (10 mL) under constant stirring at room temperature to afford a colourless solution. It was stirred for 20 minutes. It was concentrated *in vacuo*, yielding a white precipitate. The solution was decanted and the precipitate washed with anhydrous hexane and dried *in vacuo*. Yield: 1.57 g, 86%. Anal. calcd for  $\text{C}_{16}\text{H}_{36}\text{Cl}_4\text{S}_2\text{Sn}$ : C 34.8, H 6.6. Found: C 34.7, H 6.8%.  $^1\text{H}$  NMR ( $\text{CDCl}_3$ )  $\delta$ /ppm: 0.97 (t, [3H],  $\text{CH}_3$ ), 1.49 (m, [2H],  $\text{SCH}_2\text{CH}_2\text{CH}_2\text{CH}_3$ ), 1.76 (br, [2H],  $\text{SCH}_2\text{CH}_2\text{CH}_2\text{CH}_3$ ), 3.00 (vbr, [2H],  $\text{SCH}_2-$ ).  $^{13}\text{C}\{^1\text{H}\}$  NMR ( $\text{CDCl}_3$ )  $\delta$ /ppm: 13.56 ( $\text{CH}_3$ ), 21.89 ( $\text{CH}_2$ ), 30.47 ( $\text{CH}_2$ ), 43.22 ( $\text{SCH}_2$ ).  $^{119}\text{Sn}$  NMR ( $\text{CH}_2\text{Cl}_2/\text{CD}_2\text{Cl}_2$ , 298 K)  $\delta$ /ppm:  $-594$  (br),  $-603$  (br); (223 K)  $\delta$ /ppm:  $-581$  (s),  $-589$  (s). IR (Nujol)  $\nu/\text{cm}^{-1}$ : 330 (sh), 318 (s), 300 (sh) Sn–Cl.

$[\text{SnCl}_4\{\text{Bu}_2\text{Se}\}_2]$  (4). A solution of  $^n\text{Bu}_2\text{Se}$  (1.25 g, 6.45 mmol) in anhydrous hexane (5 mL) was added slowly to a solution of  $\text{SnCl}_4$  (0.840 g, 3.22 mmol) in anhydrous hexane (10 mL) under constant stirring at room temperature to afford a pale yellow solution. It was stirred for 20 minutes. It was concentrated *in vacuo*, yielding a pale orange precipitate. The solution was decanted and the precipitate washed with anhydrous hexane and dried *in vacuo*. Yield: 0.924 g, 52%. Anal. calcd for  $\text{C}_{16}\text{H}_{36}\text{Cl}_4\text{Se}_2\text{Sn}$ : C 29.71, H 5.61. Found: C 29.41, H 5.61%.  $^1\text{H}$  NMR ( $\text{CDCl}_3$ )  $\delta$ /ppm: 0.98 (t, [3H],  $\text{CH}_3$ ), 1.50 (m, [2H],  $\text{SeCH}_2\text{CH}_2\text{CH}_2\text{CH}_3$ ), 1.86 (br, [2H],  $\text{SeCH}_2\text{CH}_2-$ ), 3.10 (br, [2H],  $\text{SeCH}_2-$ ).  $^{13}\text{C}\{^1\text{H}\}$  NMR ( $\text{CDCl}_3$ )  $\delta$ /ppm: 13.48 ( $\text{CH}_3$ ), 22.83 ( $\text{CH}_2$ ), 30.42 ( $\text{CH}_2$ ), 35.64 ( $\text{SeCH}_2$ ).  $^{119}\text{Sn}$  NMR ( $\text{CD}_2\text{Cl}_2$ , 298 K)  $\delta$ /ppm:  $-717$  (br, s); (183 K)  $\delta$ /ppm:  $-719$  ( $^1J_{\text{SnSe}} = 530$  Hz, minor),  $-718$  ( $^1J_{\text{SnSe}} = 478$  Hz, major).  $^{77}\text{Se}\{^1\text{H}\}$  NMR ( $\text{CD}_2\text{Cl}_2$ , 298 K)  $\delta$ /ppm: 284 (br), 297 (br); (183 K)  $\delta$ /ppm: 299 ( $^1J_{\text{SnSe}} = 530$  Hz), 323 ( $^1J_{\text{SnSe}} = 478$  Hz). IR (Nujol)  $\nu/\text{cm}^{-1}$ : 324 (s), 302 (sh), 292 (s) Sn–Cl.

### LPCVD onto PVD $\text{SiO}_2$ substrates

Physical vapour deposited (PVD)  $\text{SiO}_2$  on Si substrates were prepared as described previously.<sup>20</sup> In a typical LPCVD experiment the reagent (70–80 mg) and PVD  $\text{SiO}_2$  substrates were loaded into a closed end silica tube in a glove box (precursor



in bulb at closed end and followed by four substrate tiles (each  $20 \times 8 \times 1$  mm) positioned adjacently along the tube). The tube was placed horizontally in the furnace such that the precursor was outside of the heated zone. The tube was evacuated to 0.02 mmHg. The furnace was then heated to the desired temperature and the temperature was allowed to stabilise. The tube was then repositioned, if necessary, to move the precursor closer to the heated zone to a point where sublimation could be observed. At this point the position of the tube was maintained until the deposition was complete (*i.e.* the precursor was completely sublimed). This typically took 1–3 hours. Once complete, the tube was allowed to cool to room temperature and transferred to the glove box where the substrates were removed and stored under  $N_2$  before characterization.

The LPCVD experiments produced black or silver films. Precursors **1** and **4** typically gave  $SnSe_2$  at all temperatures up to 1023 K. Precursor **2** gave  $SnS_2$  at all temperatures and **3** gave  $SnS_2$  at low temperatures and  $Sn_2S_3$  at higher temperatures. These results were confirmed to be reproducible. It was noted that on the occasions when precursors **1** and **2** travelled further into the heated zone,  $SnSe$  and  $SnS$  films, respectively, were obtained.

### Thin film characterisation

X-ray diffraction (XRD) patterns were collected in grazing incidence on a Rigaku SmartLab system, using  $CuK\alpha$  X-rays, a  $2\theta$  scan range of  $10$ – $80^\circ$  and an  $\omega$ -offset of  $0.7$  or  $1^\circ$ . The crystalline phase of the films was determined by matching to a literature XRD pattern<sup>22</sup> and lattice parameters calculated by further optimisation of the fit using PDXL.<sup>23</sup> Scanning electron microscopy (SEM) images and energy dispersive X-ray (EDX) measurements were obtained using a JEOL JSM 6500 F Field Emission Scanning Electron Microscope with an Oxford INCA x-sight 7418 EDX probe. An accelerating voltage of 15 kV was used and samples were calibrated against standards.

Raman scattering spectra of the deposited films were measured at room temperature on a Renishaw InVia Micro Raman Spectrometer using a helium–neon laser with a wavelength of 632.8 nm. The incident laser power was adjusted to 0.1 mW for all samples.

Van der Pauw measurements were performed at room temperature on a Nanometrics HL5500PC at 300 K. For each measurement, four copper probes with diameter of *ca.* 1 mm were carefully placed on the sample corners. Extra care was taken to ensure linear contact was obtained between each probe and the sample before each measurement.

## Results and discussion

Distorted octahedral  $tin(IV)$  halide complexes with a range of neutral thio-, seleno- and telluro-ether ligands have been reported by us previously, with the chloro complexes proving rather less hydrolytically sensitive than either those of the heavier halide analogues or indeed  $SnCl_4$  itself.<sup>24</sup> Furthermore, LPCVD studies using the selenoether complexes,

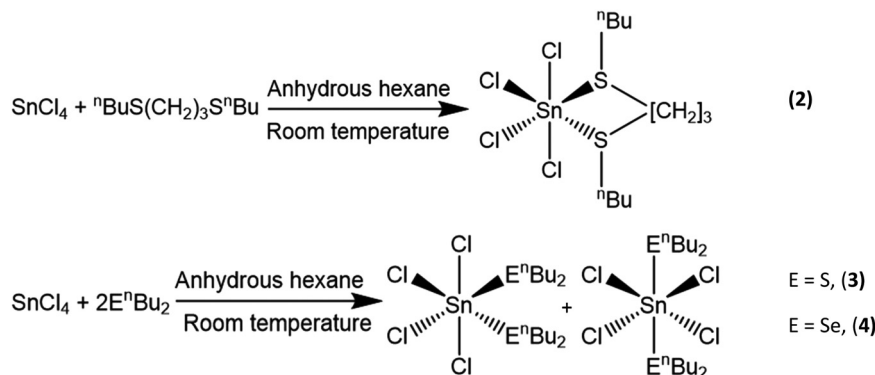
$[SnCl_4(Et_2Se)_2]^{19}$  and  $[SnCl_4(^nBuSe(CH_2)_3Se^nBu)]^{20}$  have been shown to produce polycrystalline  $SnSe_2$  thin films, whilst LPCVD of  $[SnCl_4\{o-C_6H_4(CH_2SeMe)_2\}]$  at  $600^\circ C$  resulted in  $SnSe$ ,<sup>19</sup> and, despite the S–C bonds in thioethers being stronger than Se–C bonds,<sup>25</sup>  $[SnCl_4\{o-C_6H_4(CH_2SMe)_2\}]$  has been shown to be suitable as a single source precursor for the deposition of tin sulfide thin films, forming  $SnS_2$  at  $650^\circ C$ , with some  $SnS$  forming further into the hot zone.<sup>19</sup> However, deposition of the monochalcogenides,  $SnE$  ( $E = S, Se$ ), led to rather poor, non-continuous substrate coverage in all cases, and with  $SnS_2$  typically deposited on the same substrate.<sup>19</sup> This may occur because the temperature required for the sublimation of the  $[SnCl_4\{o-C_6H_4(CH_2SMe)_2\}]$  precursor is very close to that of the boundary between deposition of  $SnS_2$  and  $SnS$ . By modifying the precursor to be more volatile, as well as incorporating  $^nBu$  substituents in place of Me groups (the former have been shown to lead to cleaner growth of metal chalcogenides in other work<sup>20</sup>), we proposed that the temperature difference between sublimation of precursor and deposition of the metal chalcogenide would be increased and better film quality achieved. Additionally, precursors containing the monodentate  $^nBu_2E$  ( $E = S, Se$ ) ligands would be more convenient to synthesise and therefore easier to access than bidentate ligands. Finally, it was anticipated that these precursors may facilitate growth of both  $SnE_2$  and  $SnE$  depending upon the deposition conditions used (with any excess  $^nBu_2E$  being distilled off readily under the low pressure CVD conditions employed or acting as a source of chalcogen to maintain stoichiometry).

The novel complexes,  $[SnCl_4(^nBu_2E)_2]$  ( $E = S, Se$ ) and  $[SnCl_4(^nBuS(CH_2)_3S^nBu)]$  were synthesized in good yield by the direct reaction of  $SnCl_4$  and the appropriate ligand in anhydrous hexane at room temperature (Scheme 1). The complexes were readily isolated as powdered solids by filtration. They are somewhat hydrolytically sensitive and therefore were stored and handled in a dry  $N_2$ -purged glove-box. They have been characterized by  $^1H$ ,  $^{13}C\{^1H\}$  and variable temperature  $^{77}Se\{^1H\}$  and  $^{119}Sn$  NMR spectroscopy, IR spectroscopy, and by microanalysis, as appropriate. The IR and microanalytical data are fully consistent with the formulations, while solution NMR data for  $[SnCl_4(^nBu_2E)_2]$  reveal similar chemical shift ranges and dynamic behaviour in solution, fully consistent with that of isomeric *cis* and *trans* distorted octahedral complexes, which could not be separated. The NMR data on  $[SnCl_4(^nBu_2E)_2]$  are very similar to those reported for  $[SnCl_4(Me_2E)_2]$ ,<sup>24,26</sup> in particular, the broad lines in the room temperature  $^{119}Sn$  and  $^{77}Se$  NMR spectra which sharpen on cooling the solutions, demonstrate rapid exchange between the two isomers as discussed in detail by Knight and Merbach.<sup>26</sup> As with the previously reported  $tin(IV)$  halide complexes with dithioether ligands,<sup>24</sup> the low temperature  $^{119}Sn$  NMR spectra from  $[SnCl_4(^nBuS(CH_2)_3S^nBu)]$  show two singlets representing the *meso* and *DL* diastereoisomers.

### Low pressure CVD experiments

Thermogravimetric analysis (TGA) of all of the precursors under an argon atmosphere showed clean and complete sub-





**Scheme 1** Preparations of the tin(IV) single source precursors used in this work.

limination of  $[\text{SnCl}_4\{\text{BuS}(\text{CH}_2)_3\text{S}^n\text{Bu}\}]$  (2),  $[\text{SnCl}_4(\text{Bu}_2\text{S})_2]$  (3) and  $[\text{SnCl}_4(\text{Bu}_2\text{Se})_2]$  (4) at 195 °C, 138 °C and 204 °C, respectively (see ESI†).

### LP CVD of tin sulfide thin films

LP CVD experiments using precursors (2) and (3) at 286 and 372 °C (0.02 mmHg), respectively, resulted in the deposition of  $\text{SnS}_2$  in both cases, without the need for an additional chalcogen source. Film deposition tended to occur mostly at the edge of the heated zone nearest to the precursor, typically leading to ca. 50% coverage of the substrate. Film properties are summarised in Table 1.

SEM images of the thin films (Fig. 1 and 2) revealed hexagonal platelets formed from both precursors, with higher uniformity and larger crystallites observed in the deposit formed from (2). In the deposition from (3), larger truncated crystallites are also observed. EDX analysis revealed composition of 36% Sn and 64% S and 34% Sn, 66% S for the films deposited from (2) (at  $T = 286$  °C) and (3) (at  $T = 372$  °C), respectively, consistent within experimental error of  $\text{SnS}_2$ , with no residual Cl observed. Grazing incidence XRD patterns also show that

crystalline  $\text{SnS}_2$  is formed in both cases, and are consistent with the space group  $P3m1$  (2H- $\text{SnS}_2$ ). In the deposition from (3), a second phase of  $\text{SnS}_2$ , in space group  $P63mc$ , is also present (4H- $\text{SnS}_2$ ) and SEM analysis shows larger truncated crystallites. The refined lattice parameters for the films deposited from (2) (Table 1) also match well with literature values of Berndtite-2H  $\text{SnS}_2$  ( $a = 3.62\text{--}3.70$ ,  $c = 5.66\text{--}5.90$  Å).<sup>12,27</sup> Lattice parameters for the two films deposited from (3) match well with those of Berndtite-2H ( $a = 3.64$ ,  $c = 5.88$  Å)<sup>28</sup> and Berndtite-4H ( $a = 3.64$ ,  $c = 11.80$  Å)  $\text{SnS}_2$ ,<sup>29</sup> respectively.

The 001 reflection is very intense in both samples, which is typical for thin films of these crystal types and indicates significant preferred orientation. Pole figure measurements were also acquired for the key reflections in the film grown from (2) in order to further investigate the preferred orientation further (Fig. 3). The pole figure for the 001 reflection reveals a sharp spot in the projection and a narrow peak in the integral at  $\alpha = 90^\circ$ . This is consistent with strong orientation of the  $c$  axis perpendicular to the substrate and the crystallites lying parallel. The SEM images show the edges of crystallites which suggests

**Table 1** Lattice parameters and resistivities measured for the tin chalcogenide thin films

Precursor	Deposition temperature/°C	Phase	Lattice parameters/Å	Resistivity/Ω cm	Reference
(1)	480–500	2H- $\text{SnSe}_2$	$a = 3.81\text{--}3.83$ $c = 6.14\text{--}6.16$	$210 \times 10^{-3}$	20
(1)	588	$\text{SnSe}$	$a = 11.459(17)$ $b = 4.166(8)$ $c = 4.433(6)$ $a = 3.664(3)$ $c = 5.935(8)$	Not measured <sup>a</sup>	This work
(2)	286	2H- $\text{SnS}_2$	$a = 3.664(3)$ $c = 5.935(8)$	2.9(9)	This work
(2)	558	$\text{SnS}$	$a = 11.19(16)$ $b = 3.98(3)$ $c = 4.24(3)$	266(3)	This work
(3)	372	2H- $\text{SnS}_2$	$a = 3.642(3)$ $c = 5.930(9)$ and	—	This work
		4H- $\text{SnS}_2$	$a = 3.643(7)$ $c = 11.84(4)$	—	
(3)	470	Mixture of $\text{SnS}_2/\text{Sn}_2\text{S}_3/\text{SnS}$	—	—	This work
(4)	325	2H- $\text{SnSe}_2$	$a = 3.8051(17)$ $c = 6.187(4)$	4.4(3)	This work

<sup>a</sup> Not measured since discontinuous film.





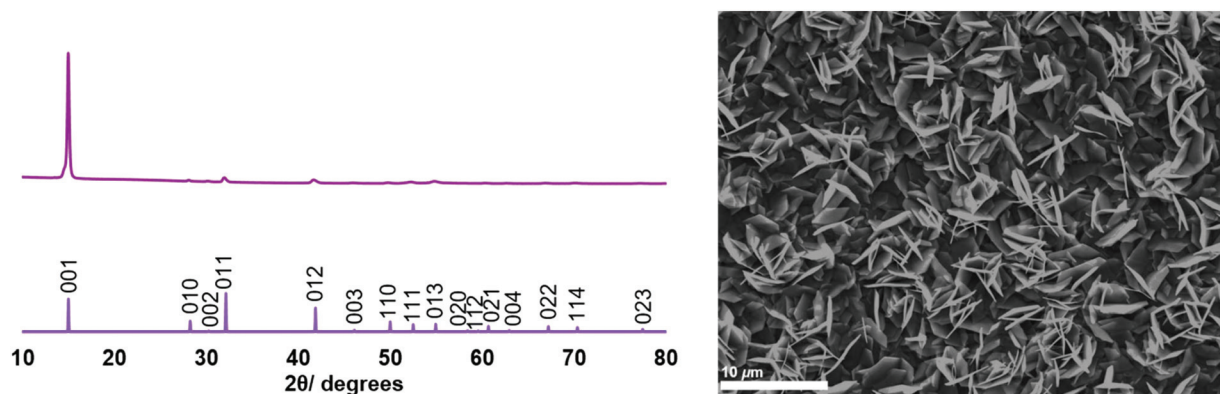


Fig. 1 (Left) Grazing incidence XRD pattern from the  $\text{SnS}_2$  film deposited from  $[\text{SnCl}_4(\text{nBuS}(\text{CH}_2)_3\text{S}'\text{nBu})]$  (2), with stick pattern from the literature data for bulk 2H- $\text{SnS}_2$ ,<sup>28</sup> (right) SEM image of  $\text{SnS}_2$  deposited from  $[\text{SnCl}_4(\text{nBuS}(\text{CH}_2)_3\text{S}'\text{nBu})]$  (2).

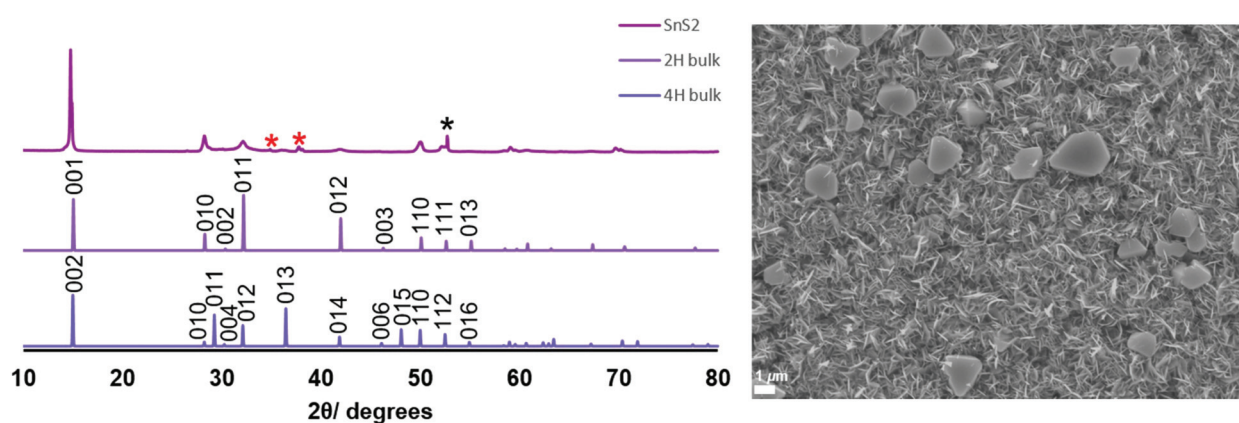


Fig. 2 (Left) Grazing incidence XRD pattern from  $\text{SnS}_2$  film deposited from  $[\text{SnCl}_4(\text{nBu}_2\text{S})_2]$  (3) and stick patterns for bulk 2H- $\text{SnS}_2$ <sup>28</sup> and 4H- $\text{SnS}_2$ .<sup>29</sup> The reflections marked \* are from the TiN layer underlying the top  $\text{SiO}_2$  on the substrate, whilst \* is from the Si; (right) SEM image of the  $\text{SnS}_2$  film grown from  $[\text{SnCl}_4(\text{nBu}_2\text{S})_2]$  (3).

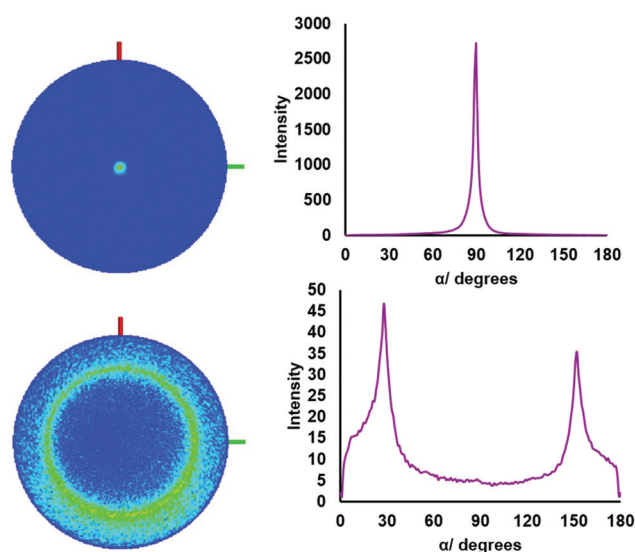


Fig. 3 3D pole figure projections with  $\alpha$  integral of the  $\text{SnS}_2$  thin film deposited from (2) at 286 °C, showing the (001) plane (top) and (011) plane (bottom) where  $\alpha$  is the tilt angle from the sample surface normal direction.

the  $c$ -axis in the film plane, so the pole figure shows the bulk of the underlying material is lying flat. For the 011 reflection, a ring is observed at  $\alpha = 30^\circ$ . The expected value for this reflection with crystallites in the  $[00l]$  orientation is calculated as  $\alpha = 27.9^\circ$  ( $\tan \alpha = a \cos 30/c$ ).

Raman spectra (Fig. 4) recorded for the thin films deposited from (2) showed an intense peak at  $\sim 320 \text{ cm}^{-1}$  and a small broad feature at  $\sim 200 \text{ cm}^{-1}$ . This is consistent with values reported in the literature of  $313 \text{ cm}^{-1}$  and  $205 \text{ cm}^{-1}$ , representing the  $A_{1g}$  and  $E_g$  modes for 2H- $\text{SnS}_2$ .<sup>30,31</sup> It is noted that an additional peak positioned at  $\sim 190 \text{ cm}^{-1}$  was also detected in some regions (red \* in Fig. 4 (left)). This is possibly the  $E_2$  peak in the 4H- $\text{SnS}_2$  phase, although this phase is not evident in the XRD data. The broad feature at  $\sim 200 \text{ cm}^{-1}$ , present in the Raman spectrum of the film deposited from (3) is attributed to the overlapping peaks ( $200\text{--}214 \text{ cm}^{-1}$ ) associated with the 4H- $\text{SnS}_2$  and 2H- $\text{SnS}_2$  phases.<sup>31</sup>

The resistivity of the  $\text{SnS}_2$  thin film grown from (2) at 286 °C was determined by van der Pauw measurements. The film shows a low resistivity,  $\rho = 2.9(9) \Omega \text{ cm}$ , compared with



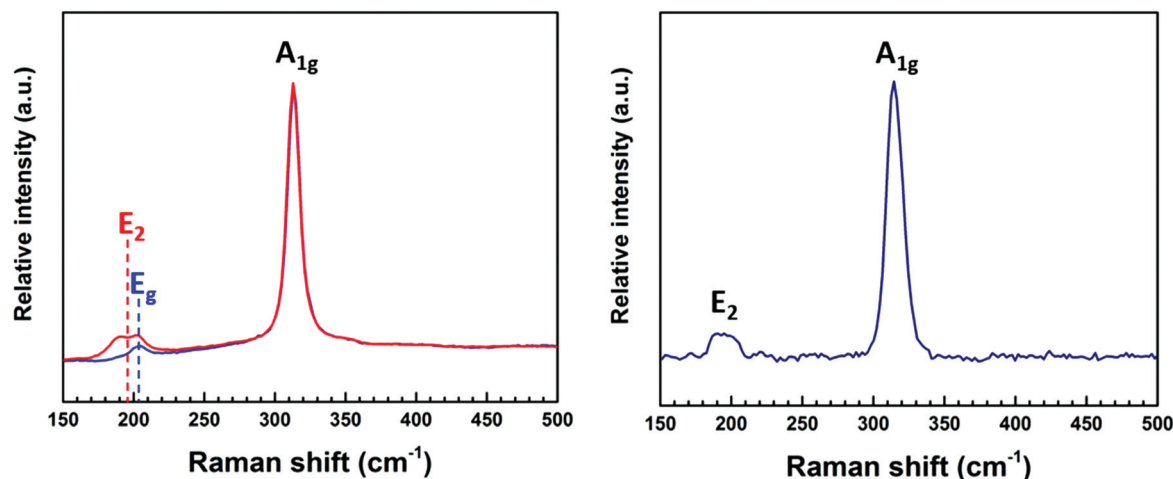


Fig. 4 Raman spectra of the  $\text{SnS}_2$  films deposited from (2) (left) and (3) (right) at  $286^\circ\text{C}$ .

other reported values.<sup>32,33</sup> This could be attributed to the deviation from precise 1:2 stoichiometry. Similar behaviour was also reported by Kourtakis *et al.* in which a low n-type resistivity of  $\rho = 4.5(5) \Omega \text{ cm}$  was observed due to a deficit of sulfur in the  $\text{SnS}_2$  film. In that case annealing in a sulfur atmosphere led to the film resistivity increasing to  $2 \times 10^5 \Omega \text{ cm}$ , demonstrating that non-stoichiometry was predominantly responsible for the low  $\text{SnS}_2$  resistivity.<sup>34</sup>

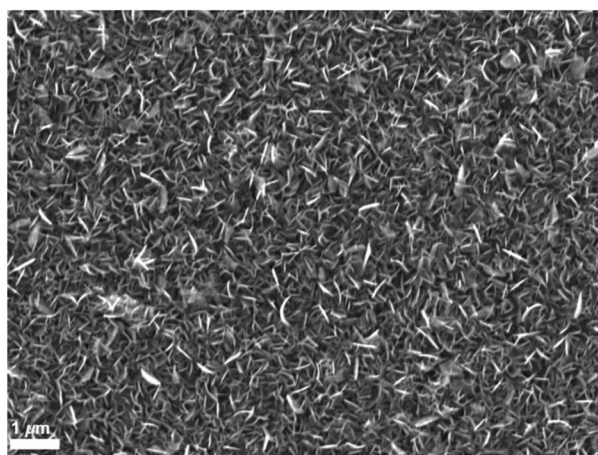


Fig. 5 SEM image of the polycrystalline  $\text{SnS}$  thin film deposited in the hotter region of the furnace ( $558^\circ\text{C}$ ) from precursor (2).

Depositions were also carried out at an increased temperature ( $558^\circ\text{C}$ ) in an effort to promote the formation of  $\text{SnS}$  over  $\text{SnS}_2$ . Using the hotter furnace temperature, LPCVD of (2) still gave mainly  $\text{SnS}_2$  (at the region nearer the precursor), but there was also evidence of some  $\text{SnS}$  formation. The morphology of the  $\text{SnS}$  film appears similar to that of  $\text{SnS}_2$  (Fig. 5), but EDX analysis show a 49%:51% Sn:S stoichiometry, within experimental error of that expected for  $\text{SnS}$  (no Cl was observed). The orthorhombic  $\text{SnS}$  phase is further confirmed by XRD analysis (Fig. 6) and the refined lattice parameters (Table 1) match well with the literature values ( $a = 11.20$ ,  $b = 3.99$ ,  $c = 4.30$ ).<sup>12</sup> The Raman spectrum (Fig. 6) of the film also clearly shows  $\text{SnS}$  with peaks at  $220$ ,  $190$  and  $165 \text{ cm}^{-1}$ . The  $165 \text{ cm}^{-1}$  peak represents the  $B_{3g}$  mode, whilst the  $190 \text{ cm}^{-1}$  and  $220 \text{ cm}^{-1}$  peaks are associated with the  $A_g$  modes and the  $290 \text{ cm}^{-1}$  peak is ascribed to the  $B_{2g}$  mode.<sup>3</sup>

The Raman spectrum (Fig. 6) of the film also clearly shows  $\text{SnS}$  with peaks at  $220$ ,  $190$  and  $165 \text{ cm}^{-1}$ . The  $165 \text{ cm}^{-1}$  peak represents the  $B_{3g}$  mode, whilst the  $190 \text{ cm}^{-1}$  and  $220 \text{ cm}^{-1}$  peaks are associated with the  $A_g$  modes and the  $290 \text{ cm}^{-1}$  peak is ascribed to the  $B_{2g}$  mode.<sup>3</sup>

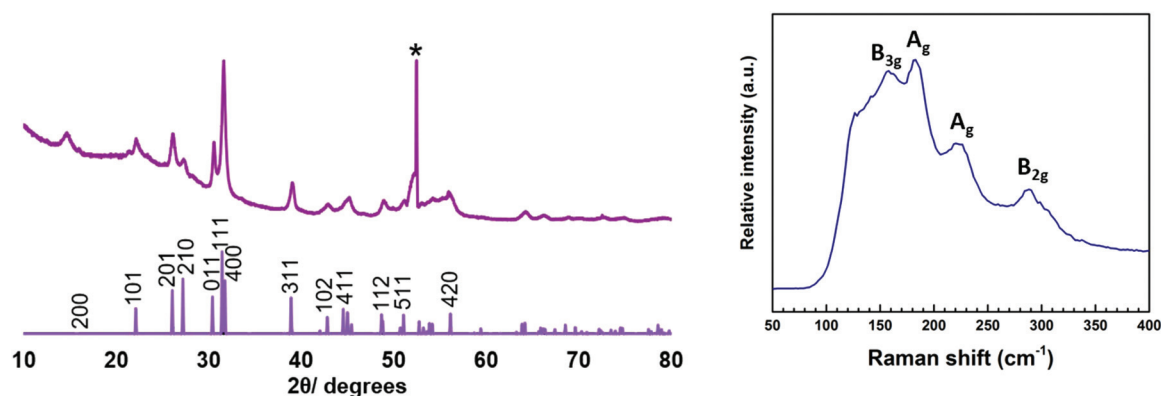


Fig. 6 XRD pattern (left) and Raman spectrum (right) of  $\text{SnS}$  deposited from precursor (2) in the hotter region of the furnace ( $558^\circ\text{C}$ ). The sharp reflection marked \* is from the Si in the substrate.





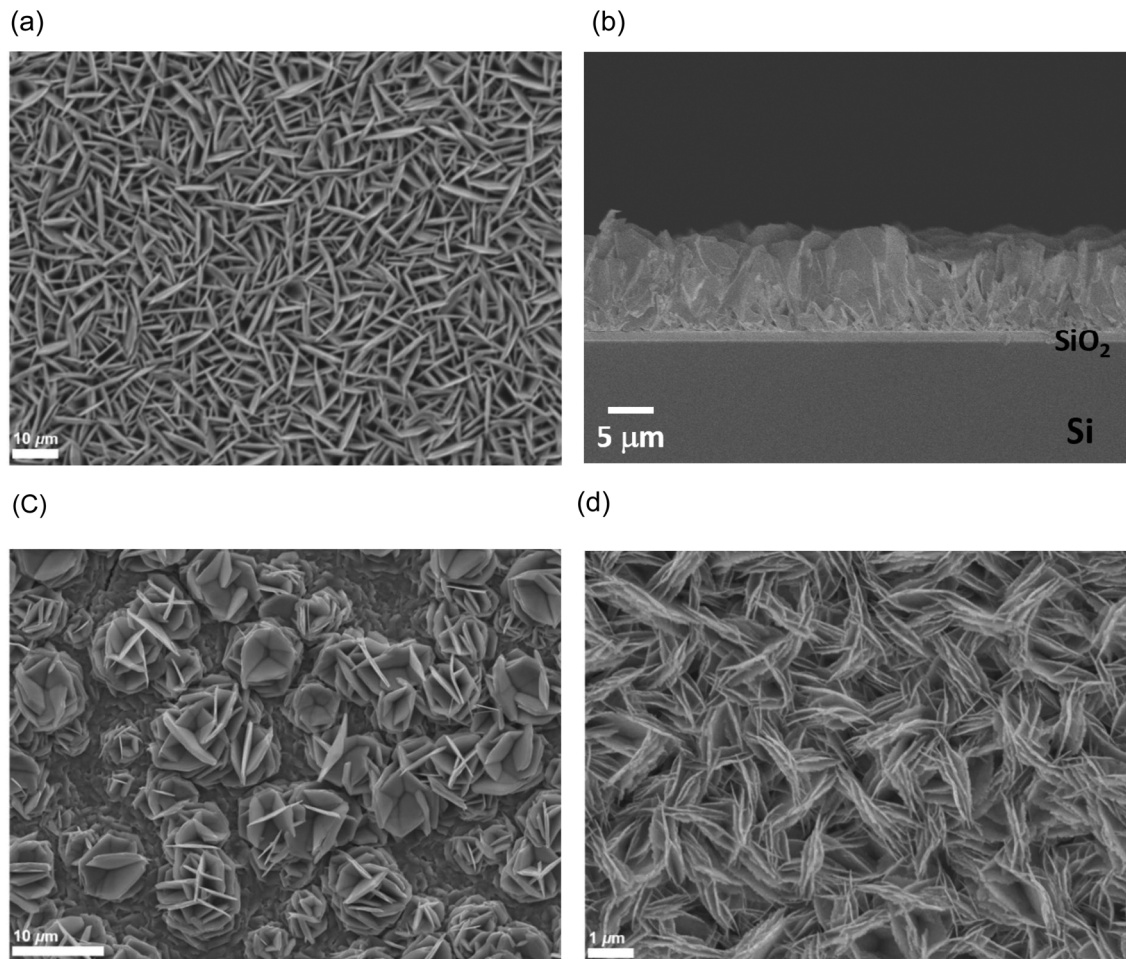


Fig. 7 SEM images of SnSe<sub>2</sub> deposited from [SnCl<sub>4</sub>(<sup>m</sup>Bu<sub>2</sub>Se)<sub>2</sub>] at 325 °C top view (a); cross section (b); a thinner region of the film deposited at 325 °C (c); top view of a SnSe<sub>2</sub> film deposited at 470 °C (d).

The SnS film deposited in this work exhibits a resistivity of 266(3) Ω cm, which is comparable to SnS films deposited *via* other techniques.<sup>35,36</sup>

In contrast, whilst SnS<sub>2</sub> films were obtained at 372 °C using precursor (3) (containing the monodentate <sup>m</sup>Bu<sub>2</sub>S ligand), LP CVD experiments at higher temperature (470 °C) resulted in mainly Sn<sub>2</sub>S<sub>3</sub> (EDX and XRD evidence, see ESI†) and this phase was observed down to 395 °C, where both SnS<sub>2</sub> and Sn<sub>2</sub>S<sub>3</sub> were observed. SEM images (ESI†) show that the crystallites of Sn<sub>2</sub>S<sub>3</sub> form clusters of small florets. However, there was also significant Cl incorporation evident from EDX analysis and the Sn:S ratio varies across the film, consistent with inhomogeneity. In the film obtained at 395 °C, several morphologies can be observed by SEM analysis and the XRD pattern obtained from this film showed a mixture of SnS, SnS<sub>2</sub> and Sn<sub>2</sub>S<sub>3</sub>.

### Tin selenide thin films

LPCVD experiments were also conducted using the tin(IV) chloride selenoether complex, [SnCl<sub>4</sub>(<sup>m</sup>Bu<sub>2</sub>Se)<sub>2</sub>] (4). At 325 °C and 470 °C, a reflective silver and a black film were obtained,

respectively. These were single phase SnSe<sub>2</sub> as identified by XRD. SEM images (Fig. 7) showed regular hexagonal platelets, typical of this space group, constituting the film deposited at

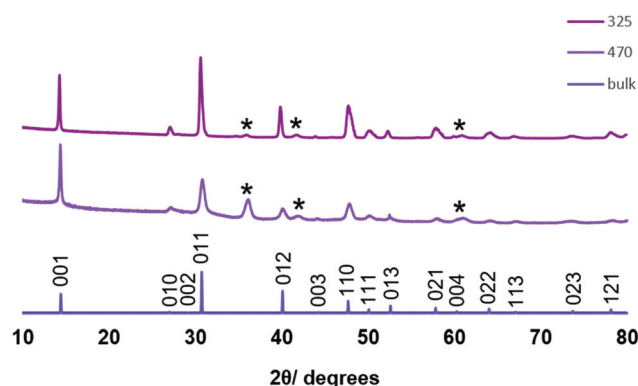


Fig. 8 Grazing incidence XRD patterns of SnSe<sub>2</sub> films deposited from [SnCl<sub>4</sub>(<sup>m</sup>Bu<sub>2</sub>Se)<sub>2</sub>] at 325 °C (top) and 470 °C (middle), together with the stick pattern from bulk SnSe<sub>2</sub> (bottom). The reflections marked \* are from crystalline TiN underlying the top SiO<sub>2</sub> layer on the substrate.



325 °C. A thinner region of this film, however, showed a more disordered morphology, and it was apparent that the platelets initially lie parallel to the substrate, before more material

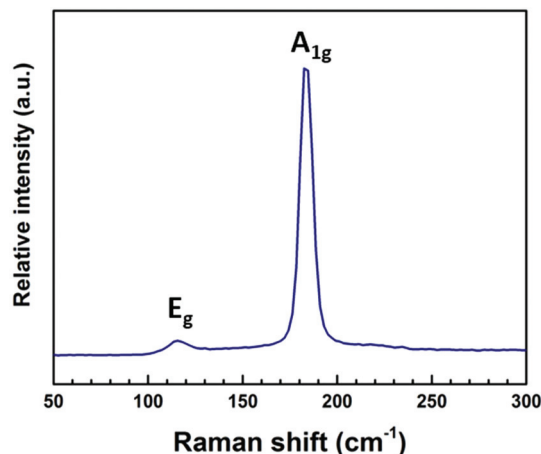


Fig. 9 Raman spectrum of SnSe<sub>2</sub> film deposited from (4) at 325 °C.

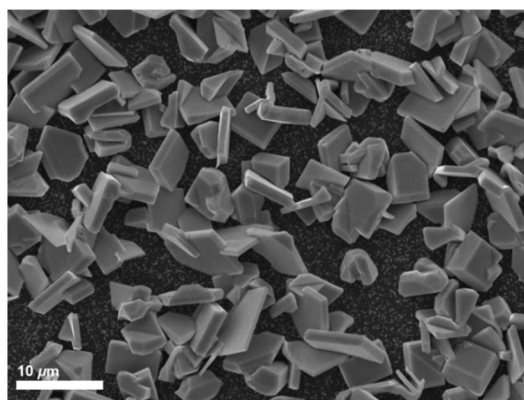


Fig. 10 SEM image of the polycrystalline SnSe deposited further into the hot zone of the furnace (at 588 °C) using precursor (1).

grows upon its surface. At an elevated temperature, the crystallites appear to be a lot smaller and rougher though still ordered. EDX analysis showed a 34 : 66 and 35 : 65 Sn : Se stoichiometry for the films deposited at 325 and 470 °C respectively. There is no evidence for incorporation of Cl into the films.

XRD analysis shows that the SnSe<sub>2</sub> crystallises in space group of  $P\bar{3}m1$  in all cases. The decrease in intensity of the 011 reflection relative to the 001 reflection (Fig. 8) suggests that the film deposited at 470 °C is thinner (and hence more strongly [001] oriented) than that deposited at 325 °C. This is borne out by cross-sectional SEM imaging and further supported by the appearance of reflections belonging to the substrate. Lattice parameters of determined for the films deposited at 325 °C and 470 °C (Table 1) are consistent with those from films deposited from our previously reported  $[\text{SnCl}_4\{\text{BuSe}(\text{CH}_2)_n\text{Se}^n\text{Bu}\}]$  ( $n = 2, 3$ ) ( $a = 3.81\text{--}3.83$  and  $c = 6.14\text{--}6.16$  Å).<sup>20</sup>

Raman spectra (Fig. 9) show an intense peak at  $185\text{ cm}^{-1}$  and a weaker feature at  $115\text{ cm}^{-1}$ . These peaks can be assigned to the A<sub>1g</sub> and E<sub>g</sub> modes of SnSe<sub>2</sub>, respectively.<sup>30</sup>

A resistivity of  $4.4(3)\text{ m}\Omega\text{ cm}$  was obtained from this SnSe<sub>2</sub> film. The value is lower than for the SnSe<sub>2</sub> films deposited *via* spin-coating and annealing ( $\sim 30\text{ m}\Omega\text{ cm}$ ),<sup>9</sup> molecular beam epitaxy ( $22\text{ m}\Omega\text{ cm}$ )<sup>8</sup> and CVD  $210\text{ m}\Omega\text{ cm}$ .<sup>20</sup> We also undertook further LPCVD studies to investigate film growth at higher temperatures using precursor (1), containing the bidentate diselenoether ligand.<sup>20</sup> Similarly to the high temperature depositions using (2) described above, these showed that increasing the furnace temperature still resulted in significant SnSe<sub>2</sub> film growth at the edge of the hot zone as before. However, where the precursor travelled further into the hotter region of the furnace, crystalline SnSe was observed. In contrast, we found no evidence for SnSe deposition using precursor (4).

The SEM images (Fig. 10) of the SnSe deposited reveal a non-continuous, orthorhombic structure. EDX analysis of the film showed a 53 : 47 Sn : Se (with no Cl evident). XRD patterns

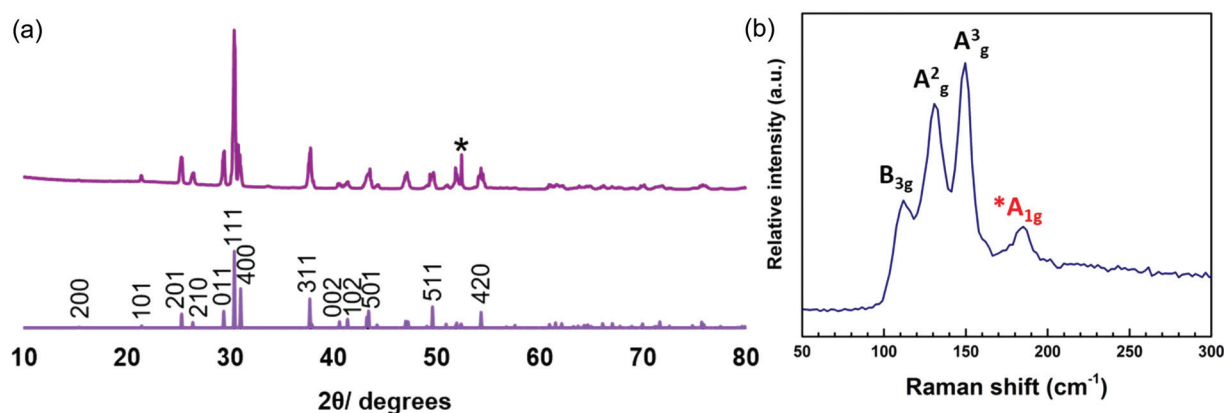


Fig. 11 XRD pattern (a) and Raman spectrum (b) of SnSe deposited from (1). The sharp reflection marked \* is from the Si underlying the SiO<sub>2</sub> on the substrate.





(Fig. 11a) show the material to be orthorhombic SnSe. The refined lattice parameters (Table 1) match well with the literature values ( $a = 11.48\text{--}11.53$ ,  $b = 4.06\text{--}4.09$ ,  $c = 4.25\text{--}4.28$ ).<sup>13</sup> The Raman spectrum (Fig. 11b) shows peaks at 150, 135 and 115  $\text{cm}^{-1}$ , consistent with SnSe. The weak band at 185  $\text{cm}^{-1}$  suggests a small  $\text{SnSe}_2$  component is present, although this is not evident in the XRD data. The peak at 115  $\text{cm}^{-1}$  can be assigned to the  $\text{B}_{3g}$  mode, 135  $\text{cm}^{-1}$  the  $\text{A}_g^2$  mode and 150  $\text{cm}^{-1}$  the  $\text{A}_g^3$  mode.<sup>37</sup> The discontinuous SnSe film coverage precluded electrical measurements.

## Conclusions

Several new molecular tin(IV) chloride complexes with monodentate and bidentate thio- and selenoether ligands bearing *n*-butyl terminal substituents have been prepared and evaluated as single source precursors for the LPCVD of both tin dichalcogenide ( $\text{Sn(IV)}$ ) and tin monochalcogenide ( $\text{Sn(II)}$ ) thin films. All four complexes have been shown to be suitable as precursors for the deposition of crystalline  $\text{SnE}_2$  thin films, the identities of which were established by grazing incidence XRD, SEM, EDX, Raman spectroscopy, and, where a single phase was obtained, van der Pauw resistivity measurements. Using higher deposition temperatures, precursors (1) and (2) have also been shown to form tin monochalcogenide thin films, which were characterised similarly. In contrast, higher temperature LPCVD experiments using the thioether complex, (3), produces multiple phases ( $\text{SnS}_2$ ,  $\text{Sn}_2\text{S}_3$ ,  $\text{SnS}$ ).

The resistivities measured for the  $\text{SnS}_2$  and  $\text{SnS}$  films are comparable to those reported for similar films produced from other deposition processes, whilst that for  $\text{SnSe}_2$  is at the lower end of the values reported.

## Conflicts of interest

There are no conflicts to declare.

## Acknowledgements

We thank STFC for funding via ST/P00007X/1, STFC and EPSRC for a CASE studentship to S. L. H. (EP/M50662X/1) and EPSRC for equipment funding (EP/K009877/1). C. G. also thanks the Royal Society for Newton Alumnus Funding.

## References

- Y. Fu, G. Gou, X. Wang, Y. Chen, Q. Wan, J. Sun, S. Xiao, H. Huang, J. Yang and G. Dai, *Appl. Phys. A*, 2017, **123**, 299.
- Y. Huang, H.-X. Deng, K. Xu, Z.-X. Wang, Q.-S. Wang, F.-M. Wang, F. Wang, X.-Y. Zhan, S.-S. Li, J.-W. Luo and J. He, *Nanoscale*, 2015, **7**, 14093.
- I. Y. Ahmet, M. S. Hill, A. L. Johnson and L. M. Peter, *Chem. Mater.*, 2015, **27**, 7680.
- F. K. Butt, M. Mirza, C. Cao, F. Idrees, M. Tahir, M. Safdar, Z. Ali, M. Tanveer and I. Aslam, *CrystEngComm*, 2014, **16**, 3470.
- M. S. Mahdi, K. Ibrahim, A. Hmood, N. M. Ahmed, F. I. Mustafa and S. A. Azzez, *Mater. Lett.*, 2017, **200**, 10.
- L.-D. Zhao, S.-H. Lo, Y. Zhang, H. Sun, G. Tan, C. Uher, C. Wolverton, V. P. Dravid and M. G. Kanatzidis, *Nature*, 2014, **508**, 373.
- C. Wang, Y. Chen, J. Jiang, R. Zhang, Y. Niu, T. Zhou, J. Xia, H. Tian, J. Hu and P. Yang, *RSC Adv.*, 2017, **7**, 16795.
- K.-M. Chung, D. Wamwangi, M. Woda, M. Wuttig and W. Bensch, *J. Appl. Phys.*, 2008, **103**, 83523.
- R. Y. Wang, M. A. Caldwell, R. G. D. Jeyasingh, S. Aloni, R. M. Shelby, H. S. P. Wong and D. J. Milliron, *J. Appl. Phys.*, 2011, **109**, 113506.
- P. Zhou, X. Wang, W. Guan, D. Zhang, L. Fang and Y. Jiang, *ACS Appl. Mater. Interfaces*, 2017, **9**, 6979.
- L. S. Price, I. P. Parkin, T. G. Hibbert and K. C. Molloy, *Chem. Vap. Deposition*, 1998, **4**, 222.
- L. S. Price, I. P. Parkin, A. M. E. Hardy, R. J. H. Clark, T. G. Hibbert and K. C. Molloy, *Chem. Mater.*, 1999, **11**, 1792.
- N. D. Boscher, C. J. Carmalt, R. G. Palgrave and I. P. Parkin, *Thin Solid Films*, 2008, **516**, 4750.
- S. L. Benjamin, C. H. de Groot, C. Gurnani, A. L. Hector, R. Huang, E. Koukharenko, W. Levason and G. Reid, *J. Mater. Chem. A*, 2014, **2**, 4865.
- R. Huang, S. L. Benjamin, C. Gurnani, Y. Wang, A. L. Hector, W. Levason, G. Reid and C. H. de Groot, *Sci. Rep.*, 2016, **6**, 27593.
- I. P. Parkin, L. S. Price, T. G. Hibbert and K. C. Molloy, *J. Mater. Chem.*, 2001, **11**, 1486.
- K. Ramasamy, V. L. Kuznetsov, K. Gopal, M. A. Malik, J. Raftery, P. P. Edwards and P. O'Brien, *Chem. Mater.*, 2013, **25**, 266.
- J. R. Brent, D. J. Lewis, T. Lorenz, E. A. Lewis, N. Savjani, S. J. Haigh, G. Seifert, B. Derby and P. O'Brien, *J. Am. Chem. Soc.*, 2015, **137**, 12689.
- S. D. Reid, A. L. Hector, W. Levason, G. Reid, B. J. Waller and M. Webster, *Dalton Trans.*, 2007, **4**, 4769.
- C. H. de Groot, C. Gurnani, A. L. Hector, R. Huang, M. Jura, W. Levason and G. Reid, *Chem. Mater.*, 2012, **24**, 4442.
- D. J. Gulliver, E. G. Hope, W. Levason, S. G. Murray, D. M. Potter and G. L. Marshall, *J. Chem. Soc., Perkin Trans. 2*, 1984, 429.
- ICSD: Inorganic Crystal Structure Database (ICSD), Fachinformationszentrum Karlsruhe (FIZ), accessed via the EPSRC funded National Chemical Database Service hosted by the Royal Society of Chemistry.
- S. Grazulis, D. Chateigner, R. T. Downs, A. F. Yokochi, M. Quiros, L. Lutterotti, E. Manakova, J. Butkus, P. Moeck and A. Le Bail, *J. Appl. Crystallogr.*, 2009, **42**, 726.
- S. E. Dann, A. R. J. Genge, W. Levason and G. Reid, *J. Chem. Soc., Dalton Trans.*, 1996, 4471; S. E. Dann, A. R. J. Genge, W. Levason and G. Reid, *J. Chem. Soc.*,



- Dalton Trans.*, 1997, 2207; A. R. J. Genge, W. Levason and G. Reid, *J. Chem. Soc., Dalton Trans.*, 1997, 4549.
- 25 L. Batt, in *The Chemistry of Organic Selenium and Tellurium compounds*, ed. S. Patai and Z. Rappoport, Wiley, NY, 1986, vol. 1, ch. 4.
  - 26 C. T. Knight and A. E. Merbach, *Inorg. Chem.*, 1985, **24**, 576.
  - 27 Y. Kumagai, L. A. Burton, A. Walsh and F. Oba, *Phys. Rev. Appl.*, 2016, **6**, 1.
  - 28 R. M. Hazen and L. W. Finger, *Am. Mineral.*, 1978, **63**, 289.
  - 29 J. R. Guenter and H. R. Oswald, *Naturwissenschaften*, 1968, **55**, 177.
  - 30 D. Walsh, S. Jandl and J. Harbec, *J. Phys. C: Solid State Phys.*, 1980, **13**, 125.
  - 31 A. J. Smith, P. E. Meek and W. Y. Liang, *J. Phys. Chem. C*, 1977, **1321**, 1321.
  - 32 A. Voznyi, V. Kosyak, A. Opanasyuk, N. Tirkusova, L. Grase, A. Medvids and G. Mezinskis, *Mater. Chem. Phys.*, 2016, **173**, 52.
  - 33 L. Amalraj, C. Sanjeeviraja and M. Jayachandran, *J. Cryst. Growth*, 2002, **234**, 683.
  - 34 K. Kourtakis, J. Di Carlo, R. Kershaw, K. Dwight and A. Wold, *J. Solid State Chem.*, 1988, **76**, 186.
  - 35 K. T. Ramakrishna Reddy, P. Purandhara Reddy, P. K. Datta and R. W. Miles, *Thin Solid Films*, 2002, **403–404**, 116.
  - 36 T. Gotoh, *Phys. Status. Solidi A*, 2016, **213**, 1869.
  - 37 S. Luo, X. Qi, H. Yao, X. Ren, Q. Chen and J. Zhong, *J. Phys. Chem. C*, 2017, **121**, 4674.

